Geochemical Journal, Vol. 46, pp. 459 to 475, 2012

Application of Laser Ablation-Inductively Coupled Plasma-Mass Spectrometry to studies of chemical diffusion, sorption, and transport in natural rock

QINHONG HU[1]* and XIANGLEI MAO[2]

[1]Department of Earth and Environmental Sciences, The University of Texas at Arlington, 500 Yates Street, Arlington, TX 76019, U.S.A.
[2]Environmental Energy Technologies Division, Lawrence Berkeley National Laboratory, University of California, 1 Cyclotron Road, MS 70-108B, Berkeley, CA 94720, U.S.A.

(*Received January 12, 2012; Accepted August 2, 2012*)

We applied laser ablation-inductively coupled plasma-mass spectrometry (LA-ICP-MS) techniques to make spatial measurements of chemical tracer concentrations in three natural rock types (tuff, sandstone, greywacke) in order to characterize important processes affecting chemical fate and transport (e.g., diffusion, sorption, imbibition, and advective transport). Specifically, we (1) evaluated LA-ICP-MS factors (e.g., spot size, laser pulse, primary grain size, and surface roughness) affecting quantitative laser sampling in both surface and depth mapping; and (2) applied LA-ICP-MS to investigate the fate and transport processes of a suite of chemicals (both nonsorbing and sorbing) in natural rock through laboratory studies of imbibition, diffusion under both saturated and unsaturated conditions, and transport in a rock core traversed by a saw-cut fracture. The results indicate that micro-scale mapping using LA-ICP-MS is a robust and sensitive technique for evaluating fate and transport of chemical species in natural rock. Direct mapping of chemical distributions using LA-ICP-MS techniques in natural rock offers distinct advantages over other methods of study, such as batch sorption experiments using crushed rock samples, and through-diffusion studies involving lengthy experiments during which test conditions may be difficult to maintain. Values of sorption distribution coefficient as determined using LA-ICP-MS techniques with centimeter-sized tuff samples, are consistently smaller, in both imbibition and diffusion experiments, than those obtained from batch-sorption tests using crushed samples with grain sizes in the 0.5–2.0 mm range.

Keywords: LA-ICP-MS, imbibition, diffusion, sorption, transport, rock

INTRODUCTION

Laser ablation refers to the process in which intense bursts of photon energy delivered by short laser pulses are used to vaporize a minute sample mass (in the range of nanograms) sample from a specific sample location. The chemical composition of the vaporized sample is then analyzed by an inductively coupled plasma-mass spectrometer (ICP-MS). Since the first experiment of Gray in 1985, laser ablation coupled with ICP-MS (LA-ICP-MS) has evolved into a powerful analytical tool for *solid* sampling and analysis (e.g., Russo *et al*., 2000, 2002, 2004; Longerich, 2008; Sylvester, 2005, 2008). LA-ICP-MS can determine, almost simultaneously, a large number of chemical elements at low detection limits, typically in the range of nanograms per gram to low-micrograms per gram.

Applications of LA-ICP-MS have been reported in a variety of environmental and geological studies for a diversity of sample types. Materials sampled have included biological specimens such as tree rings, bone, hair, teeth, seashells, fish otoliths, fish scales, and snake tail (Raith *et al*., 1996; Watmough *et al*., 1998; Veinott, 2001; Jackson *et al*., 2003; Bellotto and Miekeley, 2007; Sela *et al*., 2007; Arora *et al*., 2011), airborne particulates (Wang *et al*., 1999; Liu *et al*., 2004; Hsieh *et al*., 2011), rocks and minerals (e.g., Fryer *et al*., 1993; Jackson *et al*., 2004; Tanaka *et al*., 2007), and fluid inclusions (Shepherd and Chenery, 1995; Günther *et al*., 1998; Heinrich *et al*., 2003; Mason *et al*., 2008). However, publications on the use of LA-ICP-MS techniques to study diffusion, sorption, and transport of chemicals in natural rock are limited (Hu *et al*., 2004; Hu and Möri, 2008; Wang *et al*., 2011). The high spatial resolution (in the range of microns) achieved by a focused laser beam makes LA-ICP-MS a very attractive tool for studies of chemical fate and transport in natural rock, where the chemical may only move a very limited distance. A rock surface of millimeter scale can be directly mapped for elemental concentration, even though the distribution of the element is limited by processes such as slow diffusion and strong sorption (Hu and Möri, 2008).

*Corresponding author (e-mail: maxhu@uta.edu)

Table 1. Properties of rock samples used in this study

Rock	Source	Porosity (%)	Permeability (m^2)
Indiana Sandstone	Gas storage formation, IN	22.8	9.1×10^{-13}
Welded Tuff	Yucca Mountain, NV	9.3	5.0×10^{-19}
Meta-graywacke	The Geysers steam reservoir, CA	3.9	1.2×10^{-17}

Interest in fluid flow and chemical transport in fractured rock has grown rapidly in the past three decades, driven by the need to characterize contaminated sites, to evaluate potential sites for waste disposal or carbon sequestration, and to provide chemical transport information needed for groundwater management, geothermal energy development, or hydrocarbon recovery (Evans and Nicholson, 1987; Bear *et al*., 1993). The evaluation of processes such as the sorption of dissolved chemicals (e.g., radionuclides) by natural rock relied heavily upon batch-sorption or column-transport experiments. These often involved the use of crushed rock samples or samples sliced from solid rock; concentrations of sorbed or dissolved species were typically determined by labor-intensive extraction and analysis procedures. For example, Perkins and Lucero (2001) described an experiment in which thin layers of rock (in the range of 73 to 418 μm) were removed by milling from an intact core of Culebra dolomite collected at the Waste Isolation Pilot Plant, a nuclear waste disposal facility in New Mexico. The milled layers were examined by liquid scintillation counting to determine concentrations of ^{241}Pu (plutonium) and ^{241}Am (Americium). The objective was to obtain concentration profiles as a function of distance for these elements. However, the large spatial resolution of the milling approach produced only a few above-background data points, because of the strong retardation of ^{241}Pu and ^{241}Am with the rock matrix. In another laboratory study, Hu *et al*. (2002) examined the penetration of chemical tracers (bromide and two dyes) into unsaturated tuff collected at Yucca Mountain, Nevada. The penetration of these tracers occurred from imbibition and diffusion into tuff prepared under two different initial water saturations. The rock milling method, with 1 mm thickness resolution, allowed concentration profiles of non-sorbing bromide to be defined, but was not sufficient for delineating the distribution front of sorbing dyes.

Typically, batch-sorption experiments incorporate saturated conditions and large water/rock ratios that are not representative of *in situ* vadose zone conditions (Limousin *et al*., 2007). Crushed rock samples are used, in which the effective sample size—i.e., the grain size of the sample (in the range of microns to sub-millimeters)—is chosen more or less arbitrarily, and often primarily for reasons of experimental convenience. In addition, batch-sorption experiments typically employ well-mixed conditions that could yield large sorption values that may not apply to actual *in situ* flow conditions, which are particularly characterized by limited contact time between the fluid and intact rock. Finally, for weakly-sorbing chemicals, the batch-sorption approach can produce variable and even negative sorption values, because the methodology inherently depends on the subtraction of two numbers (initial and final aqueous concentration) that, for weakly-sorbing chemicals, may be similar. To minimize these problems, studies of chemical sorption should ideally be conducted using intact (non-crushed) rock specimens under conditions that approximate the prevailing field situation (e.g., in saturation and contact time).

In this paper, we demonstrate the application of LA-ICP-MS in laboratory studies of chemical fate and transport in natural rock. The studies included experiments involving (1) chemical imbibition, (2) saturated diffusion, (3) unsaturated diffusion, and (4) fracture flow. Our results demonstrate that LA-ICP-MS offers important advantages over other methods in environmental studies of chemical fate and transport in various rock types.

ROCK SAMPLES

Samples of three rock types were collected, representing a significant range of the petrophysical characteristics (e.g., porosity, permeability, mineralogy, and grain size) that most affect diffusion, sorption, and other transport processes. These rock types were fine-grained volcanic tuff, coarse-grained sandstone, and weakly metamorphosed graywacke (sandstone characterized by an irregular grain structure); they represent a range of environmental and economic significance (Table 1). For example, the Topopah Spring welded volcanic tuff was collected from the underground tunnel at Yucca Mountain, Nevada. Throughout the period from the late 1970's to 2008, this site was intensively studied as a potential high-level nuclear waste repository.

CHEMICALS

Many radionuclides (e.g., ^{90}Sr, ^{99}Tc, ^{129}I, ^{137}Cs, ^{237}Np, and uranium and Pu isotopes) are of concern with respect to health risks at contaminated sites associated with past

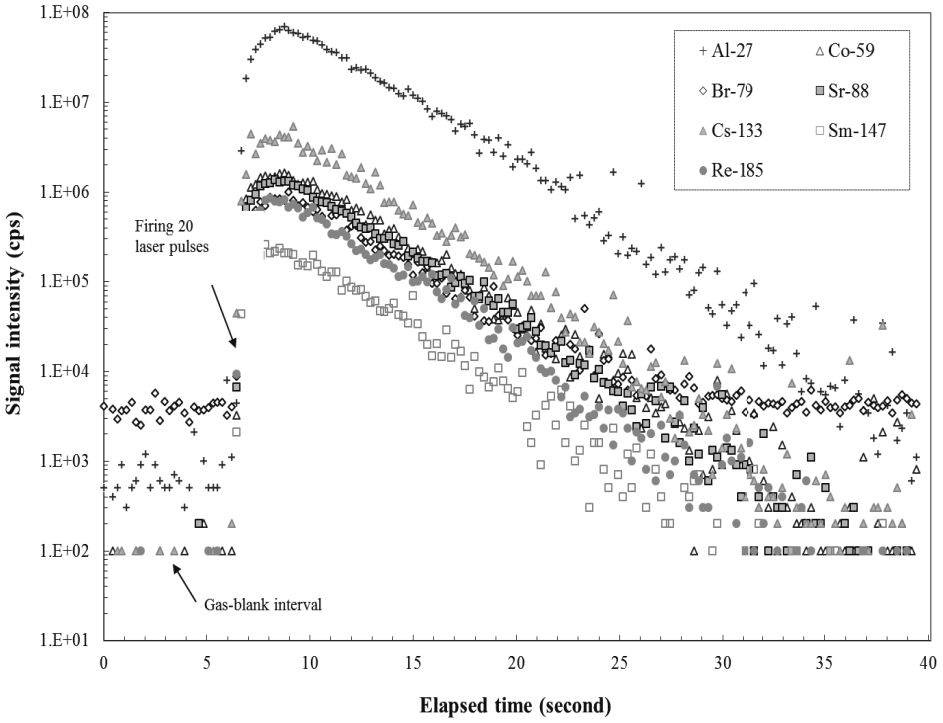

Fig. 1. Time resolved LA-ICP-MS signals for selected tracer and intrinsic elements on a tuff sample.

Table 2. List of LA-ICP-MS operating conditions

Laser ablation	
Laser system	Minilaser II, Coherent, New Infinity; Nd:YAG
Operating mmode	Q-switched
Wavelength	266 nm
Output power (mJ/pulse)	1.1–1.3
Pulse duration (ns)	6
Repetition rate (Hz)	10
Gas blank time (s)	6–10
ICP-MS	
Spectrometer	VG-PQ3
Forward power (W)	1350
Argon flow rate	
Carrier gas (l/min)	0.9
Auxiliary gas (l/min)	1.02
Cooling gas (l/min)	14.2
Dwell time per peak (ms)	varies among analytes (10–100)
Data acquisition mode	Time resolved
Acquisition duration (s)	40–70

nuclear operations, or with respect to potential risks at geological repositories for high-level nuclear wastes (Hu *et al*., 2010). In terms of chemicals, the primary focus in this study was on radionuclides, but both radionuclides and non-radioactive species were employed in the experiments to better investigate how the processes of imbibition, diffusion, sorption, and movement in fractures may affect the fate of radionuclides. Thus, non-radioactive cesium (Cs) and strontium (Sr) were selected as surrogates for radioactive ^{137}Cs and ^{90}Sr, based on their chemical similarity to these radionuclides. Similarly, perrhenate (ReO_4^-) was selected as an analog for $^{99}TcO_4^-$ (Brookins, 1986), and samarium (Sm) an analog for actinides with +3 valance state. Perhrhenate, bromide (Br^-) and/or iodide (I^-) were used as nonsorbing tracers, with their conservative behavior confirmed from previous laboratory column transport tests using crushed tuff and many other geological samples (Hu and Moran, 2005). These anionic tracers provide different aqueous molecular diffusion coefficients (Br^-/I^- versus ReO_4^-) to evaluate the importance of the diffusion process in rocks. The selected cationic sorbing tracers, including Cs^+, Co^{2+}, Sr^{2+}, Sm^{3+}, and Pu(V), were used to study delayed transport (retardation) related to cationic interactions with rock minerals. The chemical suite provided a range of sorption affinities, with Pu and Am (Sm) commonly reported to be the most strongly sorbed (Zhang and Brady, 2002).

Chemical tracer solutions were prepared using ultrapure (Type 1) water from >99% pure reagents ($CoBr_2$, CsBr, CsI, NaBr, $NaReO_4$, $SmBr_3{\cdot}6H_2O$, $SrBr_2{\cdot}2H_2O$, Aldrich Chemical Co.). Concentration levels used for the imbibition and saturated-diffusion experiments were 400 mg/L $CoBr_2$, 100 mg/L CsI, 4000 mg/L NaBr, 100 mg/L $NaReO_4$, 200 mg/L $SmBr_3$, and 400 mg/L $SrBr_2$. In the

unsaturated-diffusion experiments, higher concentrations of 5000 mg/L CsBr, 50000 mg/L NaBr, 5000 mg/L $NaReO_4$, 10000 mg/L $SmBr_3$, and 20000 mg/L $SrBr_2$ were used to pre-saturate the tracer-source tuff samples. This was done to ensure that at least a very small diffused tracer concentration (e.g., near the limit of LA-ICP-MS detection) would be achieved in the tracer-free sink tuff samples.

LA-ICP-MS Methodology

Instrumentation and data acquisition

A CETAC LSX-200 laser ablation system (CETAC Technologies) with variable spot sizes ranging from 10 μm to 300 μm, interfaced with an ICP-MS (VG-PQ3, VG Elemental) was used in the study. The CETAC laser system has a flat laser beam energy profile, and the Nd:YAG laser was operated in Q-switched mode at 266 nm wavelength with 6 ns pulse duration and a repetition rate of 10 Hz (Guillong *et al*., 2002). Typical operating conditions for the LA-ICP-MS are presented in Table 2; the dwell time per peak was 10 milli-second (ms) for most elements, and 50–100 ms for radionuclide tracers at low concentration (e.g., ^{237}Np and ^{242}Pu) and for evaluating instrument background at atomic mass-to-charge ratios of 220 or 245.

During data acquisition, signal intensities (counts per second, cps) were recorded for elements applied as tracers (e.g., ^{88}Sr, ^{133}Cs, ^{185}Re, ^{237}Np and ^{242}Pu) or intrinsic to the rock (e.g., ^{29}Si, ^{44}Ca, ^{85}Rb, ^{137}Ba, ^{232}Th). The intensity during the gas blank interval was taken as the background from isotopic- and polyatomic-mass interferences, and subtracted for the integration of the intensity after laser ablation was initiated; an Excel macro was constructed for this data reduction process. Figure 1 shows a typical result of time-resolved LA-ICP-MS signals.

The surface mapping was conducted by firing laser pulses at a sample location on the rock surface, collecting signal responses by ICP-MS, and then moving to the next sample location. A closer sampling interval was used near the tracer-contacted face (the tracer-entry face, e.g., the imbibition bottom) than on the opposite (tracer-exit) face. After mapping the exterior rock surface(s), the cubic samples used in the diffusion and imbibition tests were cracked open, using a hammer and chisel on the tracer-exit face, to expose the sample interior. Smearing of the tracer signal in this process was minimized by first covering the tracer-exit face with a Teflon film. The opened, and usually rough, interior surface was then mapped using the same surface-mapping technique, but with the laser focus adjusted anew at each sampling location to accommodate the rough surface.

In addition to the surface mapping, depth mapping was carried out to study sub-micron range chemical penetration into rock. In depth mapping, lasers are fired consecutively at the same location on the rock surface (e.g., the imbibition face) and the number of laser pulses fired (which corresponds to the sampling depth) is monitored. The laser pulses were incrementally increased until the cumulative sampling depth was on the order of several hundred microns. Depth mapping, with its micron-range spatial resolution, can normally capture even very limited distributions of tracer chemicals, such as those encountered in studies involving strongly retarded materials, and can thus provide a valuable supplement to surface-mapping results.

Spot size and laser pulse

The spot size dictates the spatial resolution during surface mapping, whereas the number of laser pulses fired determines the amount sampled. The choice of practical spot size may be dictated by the degree of heterogeneity of the matrix. However, in contrast to some geological studies (for example, the determination of the elemental composition of fluid inclusions of small sample size, e.g., 10–25 μm), studies of the fate and transport of chemical tracers in natural rock commonly involve cm-sized samples, and spatial resolutions on the order of tens of microns are sufficient for most purposes.

Selection of a large spot size can mitigate the variability arising from the differences between pore-size and grain-size of rock matrix, and better achieve representative sampling. The Yucca Mountain volcanic tuff consists largely (~99 vol. %) of a former glassy matrix, which is now devitrified to fine crystals (3–10 μm diameter) of cristobalite, alkali feldspar, and quartz (Johnson *et al*., 1998). In this work, a spot size of 100 μm was used for samples of fine-grained tuff, whereas a spot size of 200 μm was used for the coarser-grained sandstone and metagraywacke samples. For both spot sizes, measured relative standard deviations (RSD) for major intrinsic elements were about 10–15% at six randomly-chosen sampling locations.

Figure 2a shows the relationship between the ICP-MS signal responses (cps, *y*-axis) for nine elements naturally occurring in the tuff, as a function of the laser pulse numbers (*x*-axis). These elements span a wide atomic mass unit (amu) range. Without adjusting the laser focal distance, the response is linear across the amu range up to at least 100 laser pulses, corresponding to a depth of about 80 μm, as estimated from a measured 0.8 μm depth/pulse with a white-light interferometer. At greater depths, the laser begins to lose focus.

Figure 2b shows the shape and depth of a crater formed from laser ablation on a machined tuff sample with a measured surface roughness of 2.2 μm. The results show that the crater exhibits a flat bottom after 10–25 laser pulses. These findings indicate that we can correlate the number of laser pulses to the crater depth (i.e., the sam-

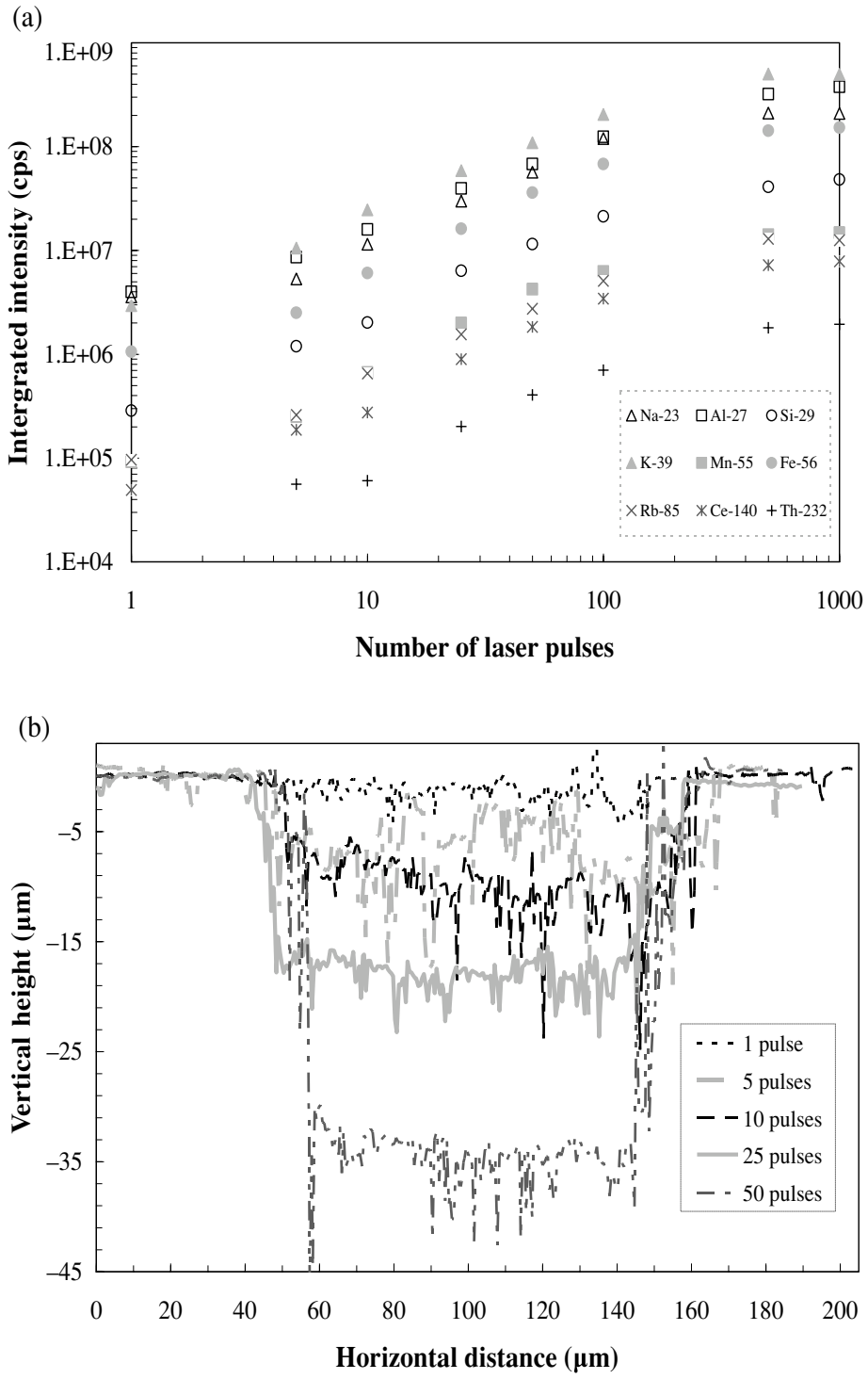

Fig. 2. (a) Linearity between responses of intrinsic tuff elements and numbers of laser pulses; (b) Crater depth and shape at a nominal 100-µm spot size; the numbers of laser pulses are indicated in the legend.

pling distance) during tracer depth-mapping of rock matrix to evaluate µm-range fate and transport processes (e.g., matrix diffusion).

For environmental studies, both surface- and depth-mapping of the chemical distribution in the rock may be necessary. However, attention should be paid to the maximum practical depth that can be achieved in depth-mapping. The crater depth-to-diameter (aspect) ratio is

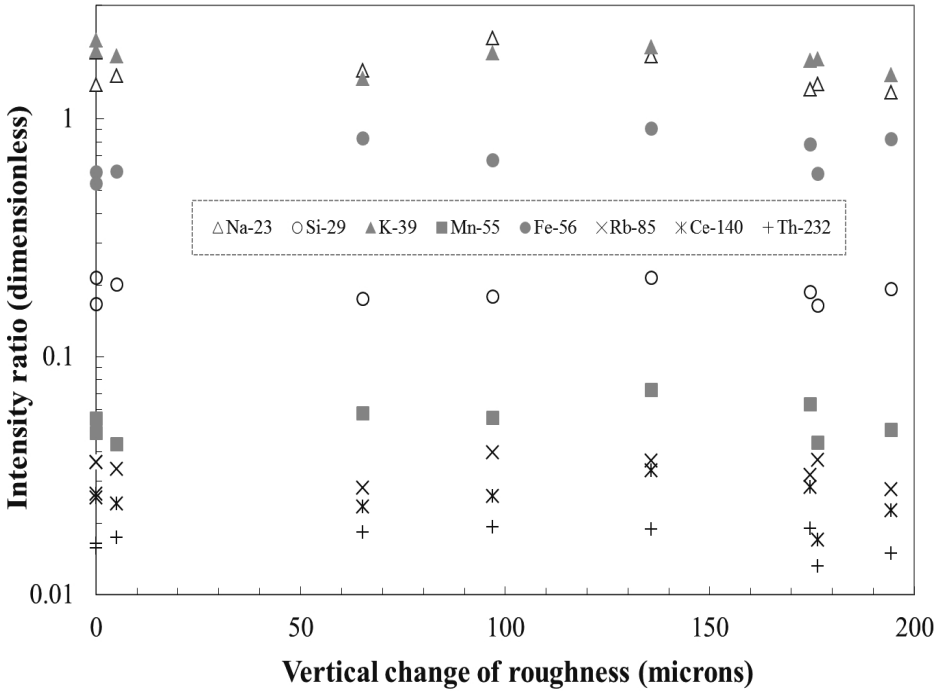

Fig. 3. Surface mapping (100-μm spot size, 20 laser pulses) of a tuff sample with a rough surface. The intensity ratio in the y-axis denotes the signal of an analyte divided by the signal of an internal standard (Al for tuff).

an important parameter determining the degree of elemental fractionation (Eggins *et al*., 1998; Borisov *et al*., 2000; Woodhead *et al*., 2008). As the aspect ratio increases, mass removal mechanisms may change from photo-thermal to plasma-dominated. As the crater deepens, the ablation rate (amount of mass removed per laser pulse) decreases. Cone-shaped craters tend to hinder in-depth profiling because the chemical carry-over in successive laser pulses may lead to an inaccurate measurement of the concentration profile with depth. The potential of redeposition of ablated materials to affect the subsequent sampling has been evaluated by several papers (cf., Woodhead *et al*., 2008), who reported that depth profiling can yield optimal results as long as the aspect ratio (depth:width) is less than 2:1. An approach that we use is to carry out shallow depth-mapping (in the range of tens of microns) to profile the distribution of strongly-sorbed chemicals, and then to perform surface-mapping of crack-opened interior surfaces (using a spot size of 100 or 250 μm) to obtain the distribution of less strongly sorbed tracers.

In research involving natural rock, samples with rough surfaces are frequently encountered. Figure 3 presents surface profiles of a tuff sample with rough (non-machined) surfaces for nine elements at a sampling interval of 1.5 mm. At each sampling location, the laser focus was adjusted to achieve clear sample image. The stable (flat) responses indicate that nearly the same volumes were sampled at each location, with vertical changes of up to 200 μm, providing increased confidence that representative solid sampling was achieved on the rough surface. An important advantage of the LA-ICP-MS method over other analytical methods (e.g., microprobe) is that little or no sample preparation is required prior to analysis, so that the smearing of chemical presence that may accompany sample preparation is avoided.

Choice of internal standards

Quantitative measurement of chemical concentration has been one of the major challenges in LA-ICP-MS analyses due to the lack of matrix-matched calibrations (Jackson, 2008). The concentration of an analyte is usually calculated from (1) the normalized ratio (the division of signal intensity for the analyte by an internal standard, e.g., Si) of both unknown and reference samples (Longerich *et al*., 1996; Ghazi *et al*., 2000; Russo *et al*., 2002) or by (2) summation of the intensity signals for major elements of rock-forming minerals to 100% (i.e., Na, Mg, Al, Si, K, Ca, Fe, Mn, and Ti) to calculate the ablation yield correction factors, which does not require the knowledge of their concentrations (Halicz and Günther, 2004; Gagnon *et al*., 2008; Liu *et al*., 2008; Peng *et al*., 2012).

The absolute chemical concentration in a rock sample may not be required in many chemical fate and transport studies, where a signal profile in some ratio format provides sufficient information on the spatial distribution of chemicals for data interpretation; this is illustrated in the present study, as discussed below.

A very uniform distribution of elemental compositions in Yucca Mountain tuff was reported by Peterman and Cloke (2002), and many minerals in tuff contain aluminum and silicon (Dobson *et al*., 2003), which makes them a good choice as an internal standard. As shown from this work, normalized signals based on Si or Al consistently exhibit the best stability among the intrinsic tuff elements. Normalization differentiates the signal reduction due to the low ablated sample amount from that associated with the small tracer concentration at this sample spot. This normalization approach helps improve data quality in surface mapping, whether the surface is rough, machined, or machined and polished. In each of these cases, the RSD of integrated net intensity shows consistent improvement between normalized and non-normalized approaches.

Further, the minerals and other constituents (weight%) in metagraywacke were reported by Persoff and Hulen (2001) with 33–41% quartz, 21–24% albite, 7–21% chlorite ($(Mg,Al,Fe)_{12}[(Si,Al)_8O_{20}](OH)_{16}$), 5–10% illite/smectite ($K_{1-1.5}Al_4[Si_{7-6.5}Al_{1-1.5}O_{20}](OH)_4$); ($(1/2Ca,Na)_{0.7}(Al,Mg,Fe)_4[(Si,Al)_8O_{20}](OH)_4{\cdot}nH_2O$), and 2–10% K-feldspar ($KAlSi_3O_8$). In our study, it was found that Si and Ca served as suitable internal standards for metagraywacke and Indiana sandstone, based on the mean standard deviation and RSD from replicate measurements.

Chemical Fate and Transport Experiments

Imbibition test

Using an approach similar to that reported by Hu *et al*. (2002), imbibition tests were carried out to investigate coupled processes of chemical sorption and transport under unsaturated conditions. This unsaturated-transport-sorption technique overcomes some shortcomings (micron-sized crushed samples and saturated conditions) of conventional batch-sorption experiments, and yields a more realistic evaluation of chemical transport in unsaturated intact rock at the centimeter scale.

Briefly, the tests were carried out by hanging, under a balance, a cm-sized rock sample (either a cube or cylinder) inside a humidity-controlled chamber. Sides of the cube samples were coated with quick-cure transparent epoxy, and the sample top was loosely foil-covered, but left with a small hole for air escape, to minimize vapor absorption from the top face. The sample bottom was submerged to a depth of about 1 mm in a reservoir of tracer-containing solution. The imbibition rate was monitored by automatically recording the sample weight change over time. After a predetermined period of time (minutes for permeable sandstones and hours for low-permeability tuff and metagraywacke), the sample was lifted out of the reservoir, frozen with liquid nitrogen, then freeze dried under –80°C and about 1 Pa for a day, and kept in dry storage at a relative humidity below 10% prior to LA-ICP-MS analysis. Tracer distribution was mapped by LA-ICP-MS on the tracer-entry and tracer-exit faces (to evaluate source concentration and to determine if the tracer front had reached the sample top, respectively). Then, after crack-opening, the tracer distribution on the interior face was mapped as a function of distance above the imbibing bottom.

Saturated diffusion test

Saturated diffusion tests were carried out on three types of rock samples, which were fully saturated with deionized water with the help of vacuum pulling. The procedure involved the use of a pulling vacuum on dry rock, and allowing the solution to invade the evacuated pore space to achieve full saturation. The sample was then placed on a Teflon mesh inside a liquid container in such a way that only the bottom portion of the sample (to minimize hydraulic head difference) was in contact with the tracer solution, which was constantly stirred using a magnetic stirrer. The tracer solution reservoir volume was on the order of 800 mL, compared to a sample pore volume of less than 1 mL; the high volume ratio was used to ensure that a constant tracer concentration would prevail in the tracer reservoir (as required to satisfy the boundary condition of the applicable mathematical solution of the diffusion equation describing the experimental procedure). The lidded container was placed inside an incubator to maintain a controlled temperature of 23°C.

A similar approach was used by Kohne *et al*. (2002) to study tracer (chloride and bromide) diffusion in soil aggregates with surface skins of different physical properties than the matrix. Kohne *et al*. (2002) monitored tracer concentration decrease in the reservoir over time to derive the diffusion coefficient of the soil sample. In the present study, the tracer concentration distribution in the rock sample was determined *in-situ* by LA-ICP-MS after a certain diffusion time, which ranged from hours to one day depending upon rock properties such as porosity and permeability. Significantly, we were able to conduct saturated diffusion experiments in less than one day, compared with days to months for conventional through-diffusion experiments (Boving and Grathwohl, 2001).

Unsaturated diffusion test

Unsaturated diffusion experiments were conducted on tuff samples under several different initial water saturations (Hu *et al*., 2004). Briefly, this was a half-

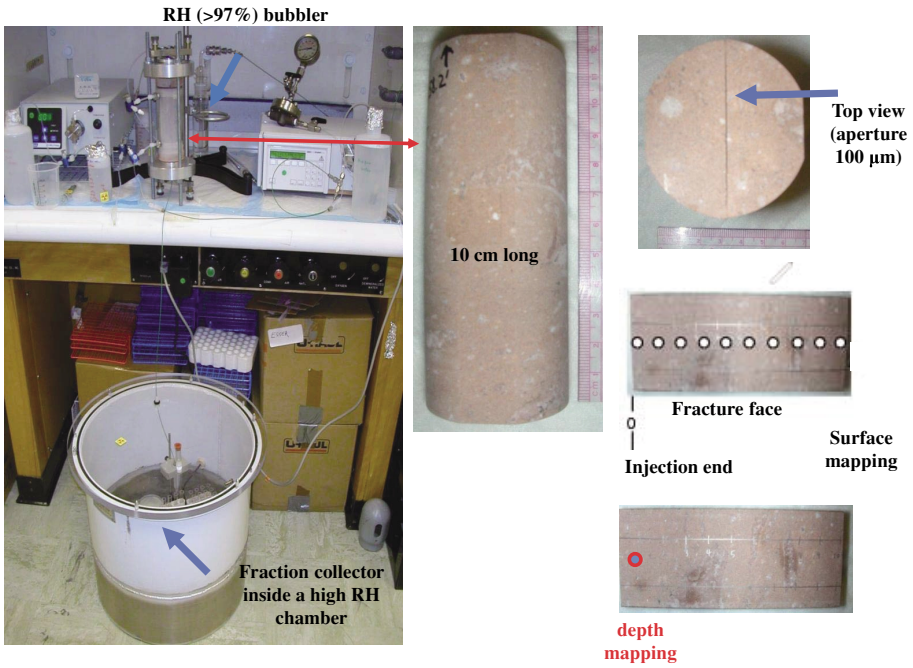

Fig. 4. Experimental setup for chemical transport study in fractured tuff core and LA-ICP-MS mapping scheme.

element (source-sink) approach, in which the source element was a cubic sample of rock initially saturated with tracer solution, the sink element a cubic or tetrahedral sample of the same rock initially saturated with deionized water, and the diffusion coefficient was determined from the final tracer distribution profile in the sink sample. The source element, a cube 1.5 cm in each dimension, was vacuum-saturated with the solution of tracer mixture; the sink element, either a cube or tetrahedron depending on the contact area to be studied, was saturated with deionized water, again with the help of vacuum pulling. Both the source- and sink-elements were next placed in an RH-controlled chamber in order to establish the same capillary potentials, thereby preventing or minimizing the opportunity for advective transport. To investigate the effect of inter-grain contact and relative humidity (hence thickness and continuity of surface water films), these experiments were designed to evaluate two configurations of sample geometry (cube-cube and cube-tetrahedron) within RH chambers with a wide range of relative humidities (43, 76, 93, 98, and nearly 100%).

Several weeks after the samples had reached a constant weight, indicating equilibrium, the source and sink elements were clamped together to start the diffusion experiments, which ranged from 0.8 to 16 days depending on the humidity environment (i.e., water saturation; the lower the saturation, the longer the duration). The samples were unclamped and separated to stop the experiments, and then frozen and freeze-dried. Tracer distributions on the exterior faces, as well as the interior surface, of both elements were mapped using LA-ICP-MS.

Fracture flow test

A liquid flow and tracer transport experiment was performed using a cylindrical tuff core (10.2 cm in length, 4.4 cm in diameter) with a longitudinal saw-cut fracture having an aperture of 100 μm (Fig. 4). The dry core was packed into a column, flushed with CO_2 to replace air in the pore spaces, and then saturated via slow pumping (0.01 mL/min) of synthetic groundwater similar to the natural groundwater of the Yucca Mountain site. The saw-cut core was then flushed with humidified air at a measured relative humidity of >97% to simulate *in situ* conditions in unsaturated rock at Yucca Mountain (Flint *et al.*, 2001).

In addition to the various radionuclides of concern (^{3}H, Br^{-}, ReO_4^{-}, I^{-}, Sr^{2+}, Cs^{+}, Sm^{3+}, ^{235}U, ^{237}Np, and ^{242}Pu), the tracer solutions used in the fracture flow transport experiments contained chemical species spanning a wide range of sorptive characteristics. ^{3}H, Br^{-}, I^{-}, and ReO_4^{-} served as non-sorbing tracers with different diffusion coefficients, to allow evaluation of the matrix diffusion contribution. A total of 100 fracture pore volumes of solution, as calculated from the cross-sectional area and aperture geometry, were directly injected into the fracture at a slow rate of 0.01 mL/min, and the core was then flushed with tracer-free synthetic groundwater at the same pumping rate. Liquid effluent from the flow column was continuously collected with a fraction collector, analyzed

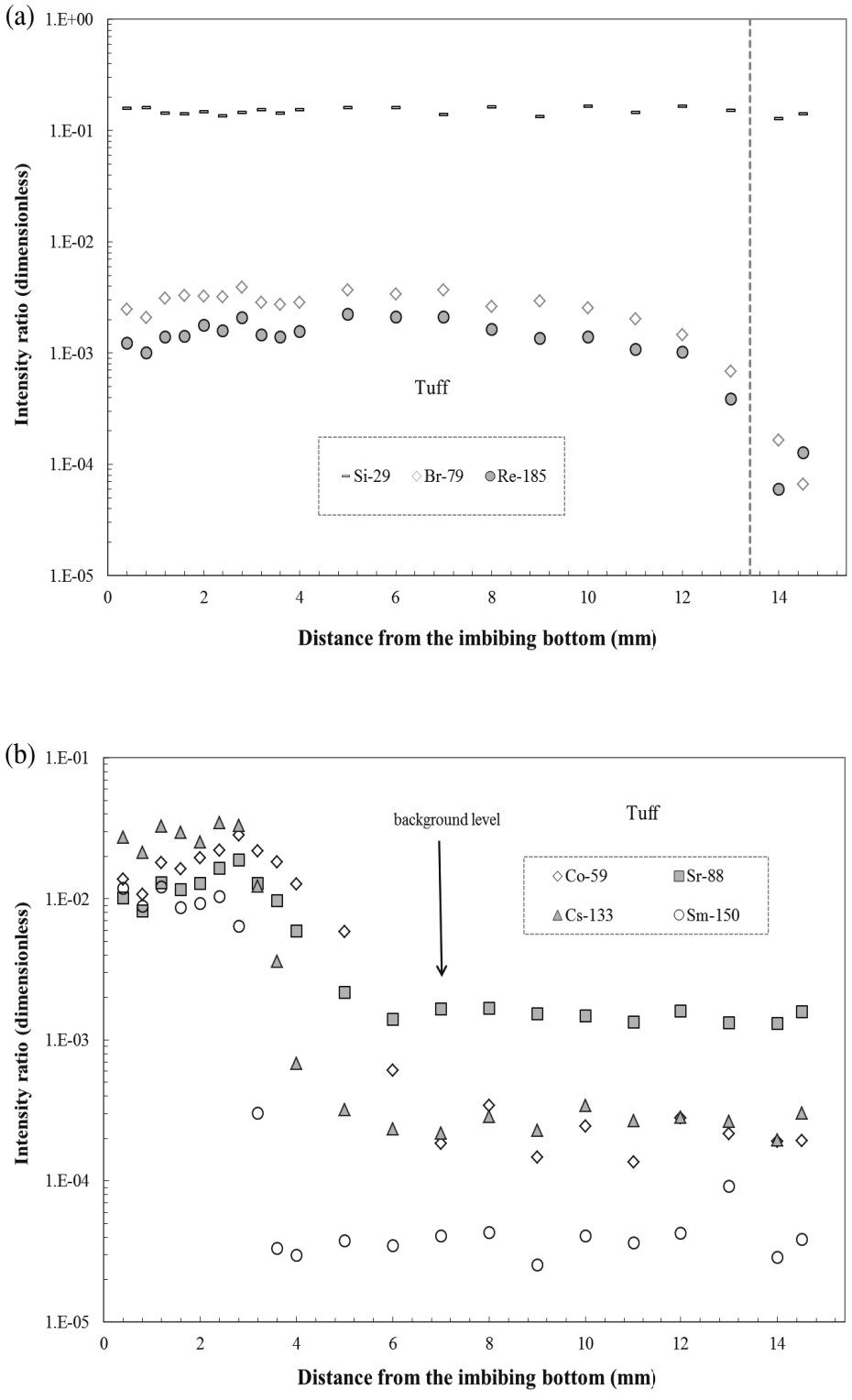

Fig. 5. Tracer distribution from surface mapping (200-μm spot size and 20 laser pulses) on the crack-opened interior face of tuff for (a) non-sorbing tracers (the vertical line indicates the distance at which the tracer concentration is half of the maximum concentration in the profile); and (b) sorbing tracers with different background levels (e.g., after 6 mm for Sm^{3+}). The intensity ratio in the y-axis is based on the internal standard of Al for tuff, and the response of another intrinsic element (Si) in tuff is also shown in (a) to indicate the stability across the sample.

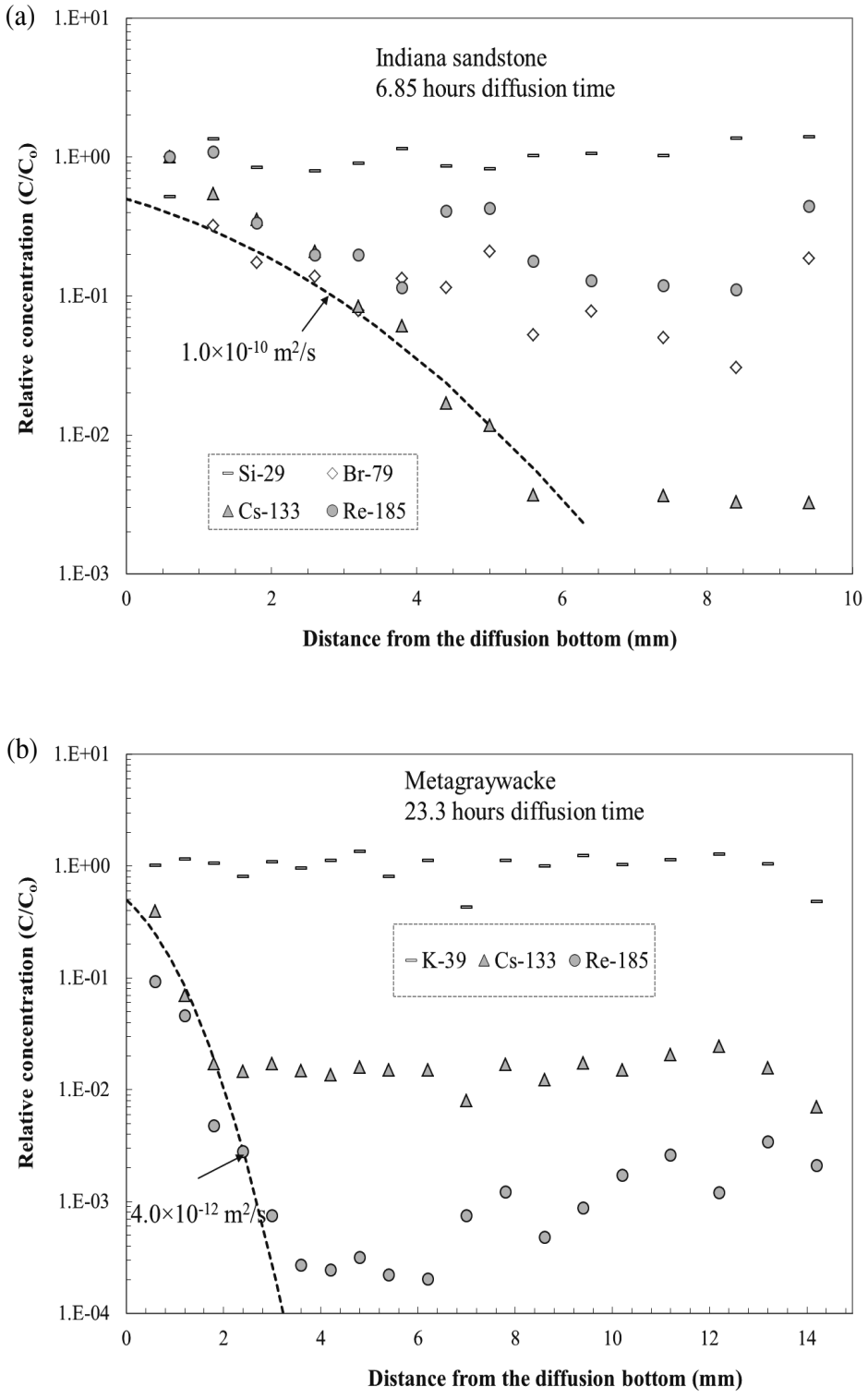

Fig. 6. Relative concentrations for anions (ReO_4^- and Br^-) and cation (Cs^+) in the saturated diffusion tests for (a) Indiana sandstone cylinder of 0.7 cm in dia., and 1.0 cm in length (Ca as the internal standard, and Si as another "uniform" intrinsic element); and (b) 1.5 cm-sized metagraywacke cube (Si as the internal standard and K as another "uniform" intrinsic element). Relative concentration in the y-axis is obtained by dividing normalized intensity ratios (analyte intensity to that of the internal standard) from the interior face to that of the diffusion bottom face, which is assumed to have the C_0 value from its continuous contact with the tracer solution. Lines in the figure are the fitted analytical diffusion solutions (Eq. (1)) for Cs^+ with the apparent diffusion coefficients shown.

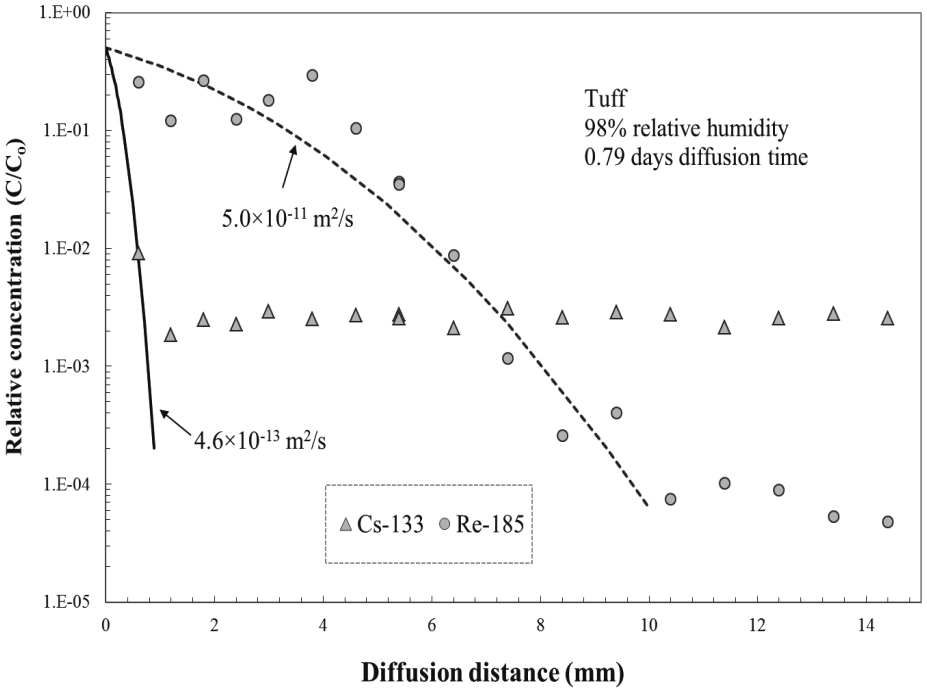

Fig. 7. Relative concentrations for ReO_4^- and Cs^+ in the sink element of unsaturated diffusion experiments conducted at 98% relative humidity environment. Lines are the fitted analytical diffusion solutions (Eq. (1)) with the apparent diffusion coefficients shown in the figure.

using ICP-MS for multiple elements, and analyzed using liquid scintillation counting for ^3H; thus the breakthrough curves of non-retarded or less-retarded tracers were obtained. To minimize the evaporation effect on effluent sample concentration from the very slow flow test, the fraction collector was placed inside a closed container in which a high relative humidity was maintained by placing several water beakers. The liquid flow experiment was 34 days in length, to allow full evaluation of the long elution process; after freeze drying of the tuff sample, the distribution of strongly retarded tracers within the tuff core was characterized using both surface- and depth-mapping by LA-ICP-MS (Fig. 4).

Results and Discussion

Chemical imbibition

In this work, transient experiments were designed to investigate water imbibition and associated chemical transport of multiple tracers into cm-scale rock. Capillary-driven imbibition acts to transport chemicals upward from the imbibing bottom face, with sorbing chemicals subject to delayed transport (retardation) compared to non-sorbing chemicals.

Figure 5 presents the tracer imbibition results for a Yucca Mountain tuff sample initially dried at 60°C. Figure 5a shows a uniform intensity distribution of the intrinsic element Si over the distance from 0 to 14.8 mm from the imbibing (bottom) surface. Figure 5a also shows nearly uniform intensity ratio distributions for the non-sorbing tracers Br^- and ReO_4^- up to ~10 mm, followed by decreasing intensities thereafter due to dispersion. These non-sorbing tracers probably reached the top boundary of 15-mm in the experimental duration of about 18 hours, as confirmed from visual observation of the wetting front reaching the sample top (tracer-exit) face. Figure 5b shows the distribution of four cationic sorbing tracers, which exhibit transport distances only up to about 4 mm. The delayed transport, compared to the non-sorbing tracers, is attributed to sorption processes, with increasing sorption according to the sequence $Co^{2+} < Sr^{2+} < Cs^+ < Sm^{3+}$. This trend generally fits the principles of surface chemistry governing cationic sorption onto surfaces, which imply a pattern of increasing sorption as follows: monovalent < divalent < trivalent (Tabatabai and Sparks, 2005). Clearly, the micro-scale LA-ICP-MS technique can interrogate the intensity distribution profiles of multiple tracer elements with different sorption coefficients.

A numerical code HYDRUS (Šimůnek *et al*., 2005), which simulates transient transport-sorption processes, is

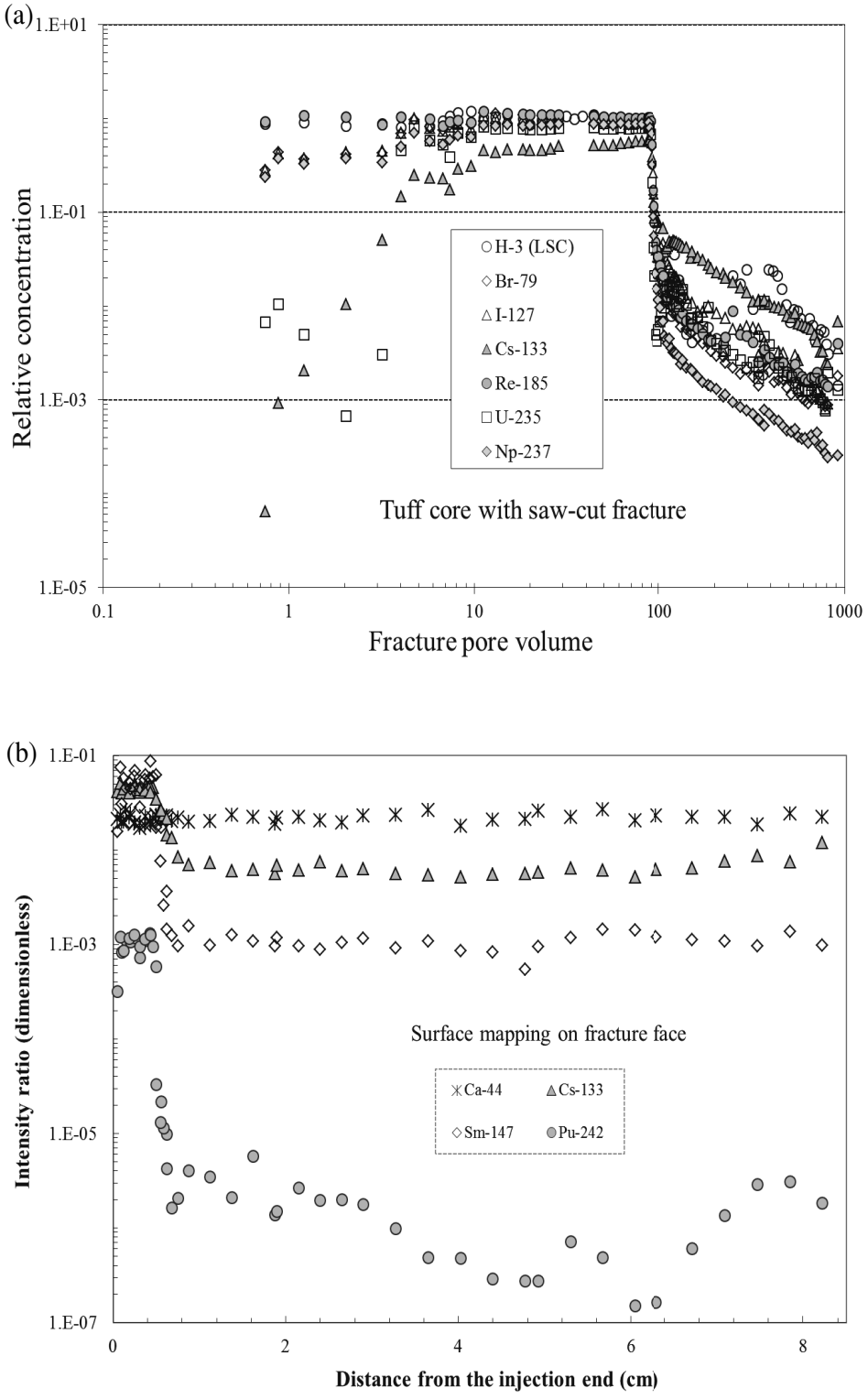

Fig. 8. Chemical transport in a fractured tuff core column: (a) effluent breakthrough curves; (b) surface-mapping results showing the distribution of strongly sorbing tracers on the fracture face of the tuff; and (c) combined depth- and surface-mapping results showing the transverse penetration of tracer chemicals into the tuff matrix from the flowing fracture at the location of 1.9 mm down from the injection end. For (a) and (b), the intensity ratio is normalized on Si and the signal response of another intrinsic element (Ca) is also shown.

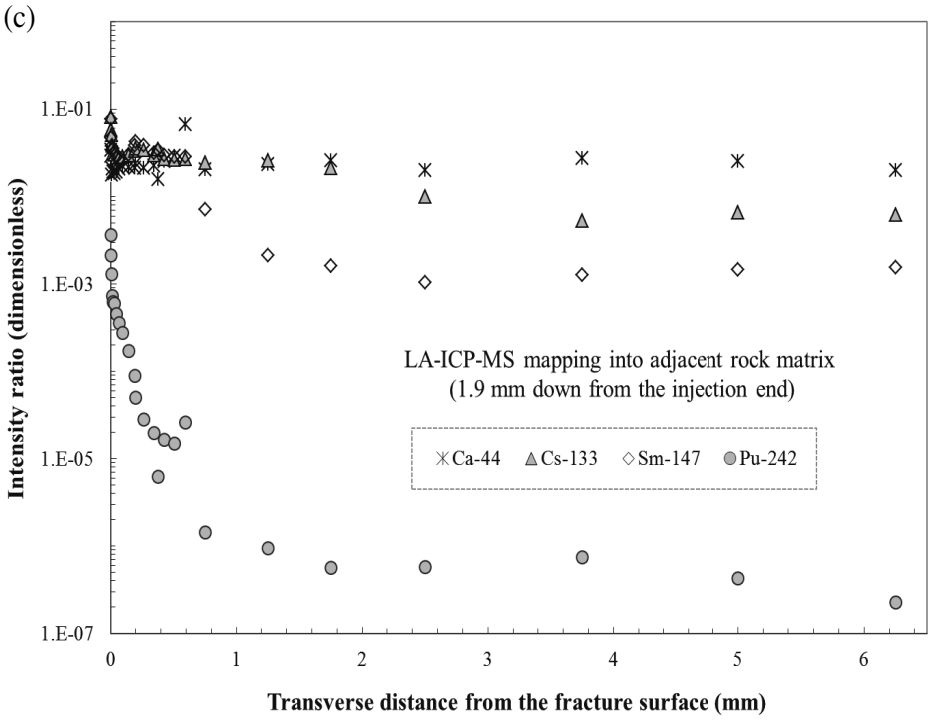

Fig. 8. (continued)

used in the analysis of experimental data to fit sorption coefficients. Concentrations of sorbed material are generally expressed as mass of sorbate per unit mass of porous-medium sorbent; concentrations of tracer remaining in the pore moisture are expressed as mass of solute per unit volume of water. The sorption distribution coefficient, K_d, is the ratio of sorbed concentration to dissolved concentration remaining in the pore water at equilibrium, and is conventionally used to characterize the tracer distribution between the aqueous and solid phases (Fetter, 2008). Values of distribution coefficient in the range of 20–31 mL/g for Sr^{2+} and 52–115 mL/g for Cs^{+} were measured from our batch-sorption tests, using crushed samples of 0.5–2 mm fraction sizes, according to standard methods (ASTM, 1998). Smaller K_d values, in the range of 5–10 mL/g for Sr^{2+} and 30 mL/g for Cs^{+} were obtained from the imbibition test reported here. These results confirm that, as discussed in the Introduction section, some of the uncertainty inherent in the batch-sorption experiments can be eliminated, and more realistic sorption data (corresponding to unsaturated transport conditions) are obtained.

Saturated diffusion

Figure 6 presents the relative concentration profiles resulting from chemical diffusion process, which were measured with LA-ICP-MS for tracers in Indiana sandstone and metagraywacke samples. For Indiana sandstone, the non-retarded tracers ReO_4^- and Br^- passed through the entire 10-mm sample length within the experiment duration of 6.8 hours (Fig. 6a). The high diffusivity implied by this result is likely related to the high porosity of the sandstone sample (Table 1). For the sorbing tracer Cs^+, the diffusion front only reached a distance of about 5.6 mm. In contrast, corresponding diffusion-test results for the metagraywacke sample (Fig. 6b) show little difference between the relative concentration profiles of ReO_4^- and Cs^+, indicating the limited chemical diffusion in metagrawacke. In the ReO_4^- diffusion profile in metagraywacke, the relative concentration decreases strongly with distance, up to a point almost 4 mm from the entry face. From that point to a distance of about 7 mm the relative concentration remains at an almost constant minimum; at distances beyond 7 mm, an increasing trend of relative concentration is observed; the causes are not known.

In a one-dimensional system in which concentration is held constant at one end and the concentration profile does not reach the opposite (diffusion exit) boundary, the analytical solution to the transient diffusion equation (Fick's second law) can be expressed as follows (Crank, 1975; Flury and Gimmi, 2002):

$$\frac{C}{C_0} = \frac{1}{2} erfc \frac{x}{2\sqrt{D_a t}} \quad (1)$$

where C (M L^{-3}) is the observed concentration at a distance x (L) from the entry boundary, C_0 (M L^{-3}) is the constant concentration at the diffusion entry boundary, D_a (L^2 T^{-1}) is the apparent diffusion coefficient incorporating both diffusion and sorption, and t (T) is the diffusion time.

Apparent diffusion coefficients were calculated from Eq. (1) using the observed relative concentration values. The results are 1.0×10^{-10} m^2/s for Cs^+ in Indiana sandstone and 4.0×10^{-12} m^2/s for ReO_4^- and Cs^+ in metagraywacke. These results illustrate the utility of LA-ICP-MS in studies of slow diffusive-sorptive transport involving multiple tracers. The experimental time periods, generally less than a day required for this approach, offer obvious advantages over the long experimental durations (days to months) often required in conventional through-diffusion approaches, particularly where the test conditions are difficult to maintain over long periods.

Unsaturated diffusion

The unsaturated diffusion experiments allowed apparent diffusion coefficients to be determined for a mixture of chemical tracers in Yucca Mountain tuff. Figure 7 shows an example of tracer relative concentration profiles obtained for ReO_4^- and Cs^+ using the cube-cube configuration in partially-saturated tuff under 98% relative humidity. Curve-fitting of Eq. (1) to the concentration profiles indicates two orders of magnitude difference in the apparent diffusion coefficients between ReO_4^- (5.0×10^{-11} m^2/s) and Cs^+ (4.6×10^{-13} m^2/s), indicating the contribution from sorption of cationic Cs^+ to its slow diffusion. The half-element approach and micro-scale LA-ICP-MS mapping made it feasible to evaluate the diffusion processes of both nonsorbing and sorbing tracers in unsaturated rock.

The measured diffusion coefficient in fully-saturated (100%) tuff for ReO_4^- is 2×10^{-10} m^2/s, compared to a value of 5.0×10^{-11} m^2/s obtained in the unsaturated diffusion experiments with the tuff saturation of 88.8%. Thus a relatively slight reduction in saturation leads to a decrease of diffusion coefficient with by a factor of 4, further illustrating the strong effect of water saturation on chemical diffusion (Hu *et al*., 2004).

From the measured diffusion coefficients, the retardation factor R_f is calculated to be 153 for Cs^+, based on tortuosity obtained from ReO_4^- profile and aqueous diffusion coefficients for Cs^+. The value of R_f is related to K_d by:

$$R_f = 1 + \frac{K_d \rho_b}{\theta}. \qquad (2)$$

This equation indicates that solute retardation is inversely related to the water content θ (dimensionless) and positively to the bulk density ρ_b (M L^{-3}). Note that the concept of K_d implicitly denotes a linear equilibrium sorption behavior (e.g., Fetter, 2008). Using the measured water content of 0.0826 and bulk density ρ_b of 2.27 g/cm^3, the K_d value can be calculated from the R_f given above to be 5.53 mL/g for Cs^+ in Yucca Mountain tuff, which is also smaller than the value of 52–115 mL/g obtained from the batch-sorption tests.

Fracture flow

Chemical transport in unsaturated fractured tuff (a tuff core with a saw-cut fracture) is characterized by rapid flow and chemical transport through the fracture, and the concomitant transverse diffusion and imbibition into the matrix (Fig. 8). This is evident from the long tailing of the non-sorbing tracers (^3H, Br^-, I^-, and ReO_4^-) in the elution portion of the experiment (Fig. 8a). Although displaying some breakthrough due to fast flow through the fracture (Fig. 8a), the strongly-sorbing tracers (Cs^+, Sm^{3+}, and ^{242}Pu) are largely sorbed onto the surfaces of the fracture within the first 0.5 cm distance from the injection face (Fig. 8b). In addition to adsorption, transverse penetration (matrix diffusion and imbibition) into the adjacent tuff matrix leads to further retardation of dissolved chemical along the fracture, and increased tracer mass held in the matrix. This is especially evident for the high-mass tracer ^{242}Pu; its presence as measured by combined μm-range depth- and surface-mapping yields an intensity ratio profile of nearly four orders of magnitude above its background ratio of 10^{-6} at the location of 1.9 mm below the injection end (Fig. 8c).

SUMMARY

The results of this paper illustrate the utility of the LA-ICP-MS approach in studies of chemical fate and transport in natural rock, particularly as associated with the processes of imbibition, saturated diffusion, unsaturated diffusion, and fracture flow. The sensitivity of the method, its extremely refined scale of measurement, and the ease with which it can be coupled to other procedures offer advantages over other approaches to the study of chemical fate and transport in solid rock. In chemical imbibition tests, the method overcomes the shortcomings of batch-sorption approaches through direct monitoring of sorbed tracers in intact and unsaturated rock. In diffusion testing, direct mapping of tracer profiles significantly reduces the experimental duration, compared with that required in through-diffusion approaches. In a transport test in a core with a saw-cut fracture, although rapid transport and early breakthrough due to flow through the fracture was of course observed, the LA-ICP-MS method revealed detailed information on the processes of transverse matrix diffusion and imbibition, which act to retard overall chemical transport.

Acknowledgments—The financial support for this work was partially provided by the University of Texas at Arlington, and by the Department of Energy (DOE) to the Ernest Orlando Lawrence Berkeley National Laboratory through the U.S. DOE Contract No. DE-AC03-76SF00098.

REFERENCES

Arora, M., Hare, D., Austin, C., Smith, D. R. and Doble, P. (2011) Spatial distribution of manganese in enamel and coronal dentine of human primary teeth. *Sci. Total Environ.* **409**, 1315–1319.

ASTM (American Society for Testing and Materials) (1998) Standard test method for 24-hour batch-type measurement of contaminant sorption by soils and sediments (D4646-87). Annual Book of ASTM Standards. American Society for Testing and Materials, Philadelphia, PA, 04.08:44–47.

Bear, J., Tsang, C. F. and De Marsily, G. (eds.) (1993) *Flow and Contaminant Transport in Fractured Rock*. Academic Press, San Diego, CA, 560 pp.

Bellotto, V. R. and N. Miekeley (2007). Trace metals in mussel shells and corresponding soft tissue samples: A validation experiment for the use of Perna perna shells in pollution monitoring. *Anal. Bioanal. Chem.* **389**, 769–776.

Borisov, O. V., Mao, X. L. and Russo, R. E. (2000) Effects of crater development on fractionation and signal intensity during laser ablation inductively coupled plasma mass spectrometry. *Spectrochim. Acta, Part B* **55**, 1693–1704.

Boving, T. B. and Grathwohl, P. (2001) Tracer diffusion coefficients in sedimentary rocks: correlation to porosity and hydraulic conductivity. *J. Contam. Hydrol.* **53**, 85–100.

Brookins, D. G. (1986) Rhenium as analog for fissiogenic technetium: Eh-pH diagram (25°C, 1 bar) constraints. *Appl. Geol.* **1**, 513–517.

Crank, J. (1975) *The Mathematics of Diffusion*. 2nd ed., Oxford University Press Inc., New York, 414 pp.

Dobson, P. F., Kneafsey, T. J., Sonnenthal, E. L., Spycher, N. and Apps, J. A. (2003) Experimental and numerical simulation of dissolution and precipitation: implications for fracture sealing at Yucca Mountain, Nevada. *J. Contam. Hydrol.* **62–63**, 459–476.

Eggins, S. M., Kinsley, L. P. J. and Shelley, J. M. G. (1998) Deposition and element fractionation processes during atmospheric pressure laser sampling for analysis by ICP-MS. *Appl. Surf. Sci.* **127–129**, 278–286.

Evans, D. D. and Nicholson, T. J. (eds.) (1987) *Flow and Transport through Unsaturated Fractured Rock*. American Geophysical Union Monograph 42, 187 pp.

Fetter, C. W. (2008) *Contaminant Hydrogeology*. 2nd ed., Waveland Press, Inc., Long Grove, IL.

Flint, A. L., Flint, L. E., Bodvarsson, G. S., Kwicklis, E. M. and Fabryka-Martin, J. (2001) Evolution of the conceptual model of unsaturated zone hydrology at Yucca Mountain, Nevada. *J. Hydrol.* **247**, 1–30.

Flury, M. and Gimmi, T. F. (2002) Solute diffusion. *Methods of Soil Analysis. Part 4—Physical Methods* (Dane, J. H. and Topp, G. C., eds.), 1323–1351, Soil Sci. Soc. Am., Madison, Wisconsin.

Fryer, B. J., Jackson, S. E. and Longerich, P. (1993) The application of laser ablation microprobe-inductively coupled plasma mass spectrometry (LA/ICP-MS) to *in situ* (U)–Pb geochronology. *Chem. Geol.* **109**, 1–8.

Gagnon, J. E., Fryer, B. J., Samson, I. M. and Williams-Jones, A. E. (2008) Quantitative analysis of silicate certified reference materials by LA-ICP-MS with and without an internal standard. *J. Anal. At. Spectrom.* **23**, 1529–1537.

Ghazi, A. M., Shuttleworth, S., Angulo, S. J. and Pashley, D. H. (2000) New applications for laser ablation high resolution ICP-MS (LA-HR-ICP-MS): Quantitative measurements of gallium diffusion across human root dentin. *J. Anal. At. Spectrom.* **15**, 1335–1341.

Gray, A. (1985) Solid sample introduction by laser ablation for inductively coupled plasma source mass spectrometry. *Analyst* **110**, 551–556.

Guillong, M., Horn, I. and Günther, D. (2002) Capabilities of a homogenized 266 nm Nd:YAG laser ablation system for LA-ICP-MS. *J. Anal. At. Spectrom.* **17**, 8–14.

Günther, D., Audetat, A., Frischknecht, R. and Heinrich, C. A. (1998) Quantitative analysis of major, minor and trace elements in fluid inclusions using laser ablation-inductively coupled plasma-mass spectrometry. *J. Anal. At. Spectrom.* **13**, 263–270.

Halicz, L. and Günther, D. (2004) Quantitative analysis of silicates using LA-ICP-MS with liquid calibration. *J. Anal. At. Spectrom.* **19**, 1539–1545.

Heinrich, C. A., Pettke, T., Halter, W. E., Aigner-Torres, M., Audetat, A., Gunther, D., Hattendorf, B., Bleiner, D., Guillong, M. and Horn, I. (2003) Quantitative multi-element analysis of minerals, fluid and melt inclusions by laser-ablation inductively-coupled-plasma mass-spectrometry. *Geochim. Cosmochim. Acta* **67**, 3473–3497.

Hsieh, Y.-K., Chen, L.-K., Hsieh, H.-F., Huang, C.-H. and Wang, C.-F. (2011) Elemental analysis of airborne particulate matter using an electrical low-pressure impactor and laser ablation/inductively coupled plasma mass spectrometry. *J. Anal. At. Spectrom.* **26**, 1502–1508.

Hu, Q. H. and Moran, J. E. (2005) Simultaneous analyses and applications of multiple fluorobenzoate and halide tracers in hydrologic studies. *Hydrol. Proc.* **19**, 2671–2687.

Hu, Q. H. and Möri, A. (2008) Radionuclide transport in fracture-granite interface zones. *Phys. Chem. Earth* **33**, 1042–1049.

Hu, Q. H., Kneafsey, T., Trautz, R. C. and Wang, J. S. Y. (2002) Tracer penetration into welded tuff matrix from flowing fractures. *Vadose Zone J.* **1**, 102–112.

Hu, Q. H., Kneafsey, T. J., Wang, J. S. Y., Tomutsa, L. and Roberts, J. J. (2004) Characterizing unsaturated diffusion in porous tuff gravels. *Vadose Zone J.* **3**, 1425–1438.

Hu, Q. H., Weng, J. Q. and Wang, J. S. (2010) Anthropogenic radionuclides in the environment. *J. Environ. Radioact.* **201**, 426–437.

Jackson, B. P., Hopkins, W. A. and Baionno, J. (2003) Laser ablation-ICP-MS analysis of dissected tissue: A conservation-minded approach to assessing contaminant exposure. *Environ. Sci. Technol.* **37**, 2511–2515.

Jackson, S. E. (2008) Calibration strategies for elemental analysis by LA-ICP-MS. *Laser-Ablation-ICP-MS in the Earth Sciences: Current Practices and Outstanding Issues*

(Sylvester, P., ed.), vol. 40, 169–188, Mineralogical Association of Canada.

Jackson, S. E., Pearson, N. J., Griffin, W. L. and Belousova, E. A. (2004) The application of laser ablation-inductively coupled plasma-mass spectrometry to *in situ* U–Pb zircon geochronology. *Chem. Geol.* **211**, 47–69.

Johnson, J. W., Knauss, K. G., Glassley, W. E., DeLoach, L. D. and Thompson, A. F. B. (1998) Reactive transport modeling of plug-flow reactor experiments: quartz and tuff dissolution at 240°C. *J. Hydrol.* **209**, 81–111.

Kohne, J. M., Gerke, H. H. and Kohne, S. (2002) Effective diffusion coefficients of soil aggregates with surface skins. *Soil Sci. Soc. Amer. J.* **66**, 1430–1438.

Limousin, G., Gaudet, J. P., Charlet, L., Szenknect, S., Barthes, V. and Krimissa, M. (2007) Sorption isotherms: A review on physical bases, modeling and measurement. *Appl. Geochem.*, **22**, 249–275.

Liu, C., Mao, X. L., Mao, S. S., Zeng, X., Greif, R. and Russo, R. E. (2004) Nanosecond and ferntosecond laser ablation of brass: Particulate and ICP-MS measurements. *Anal. Chem.* **76**, 379–383.

Liu, Y. S., Hu, Z. C., Gao, S., Gunther, D., Xu, J., Gao, C. G. and Chen, H. H. (2008) In situ analysis of major and trace elements of anhydrous minerals by LA-ICP-MS without applying an internal standard. *Chem. Geol.* **257**, 34–43.

Longerich, H. P. (2008) Laser ablation-inductively coupled plasma-mass spectrometry: An introduction. *Laser-Ablation-ICP-MS in the Earth Sciences: Current Practices and Outstanding Issues* (Sylvester, P., ed.), vol. 40, 1–18, Mineralogical Association of Canada.

Longerich, H. P., Jackson, S. E. and Günther, D. (1996) Laser ablation inductively coupled plasma mass spectrometric transient signal data acquisition and analyte concentration calculation. *J. Anal. At. Spectrom.* **9**, 899–904.

Mason, P. D., Nikogosian, I. K. and van Bergen, M. J. (2008) Major and trace element analysis of melt inclusions by laser ablation-ICP-MS. *Laser-Ablation-ICP-MS in the Earth Sciences: Current Practices and Outstanding Issues* (Sylvester, P., ed.), vol. 40, 219–240, Mineralogical Association of Canada.

Peng, S., Hu, Q. H., Ewing, R. P., Liu, C. X. and Zachara, J. M. (2012) Quantitative 3-D elemental mapping by LA-ICP-MS for basalt at the Hanford 300 Area Site. *Environ. Sci. Technol.*, **46**, 2025–2032.

Perkins, W. G. and Lucero, D. A. (2001) Interpretation of actinide-distribution data obtained from non-destructive and destructive post-test analyses of an intact-core column of Culebra dolomite. *J. Contam. Hydrol.* **47**, 107–116.

Persoff, P. and Hulen, J. B. (2001) Hydrologic characterization of reservoir metagraywacke from shallow and deep levels of The Geysers vapor-dominated geothermal system, California, USA. *Geothermics* **30**, 169–192.

Peterman, Z. E. and Cloke, P. L. (2002) Geochemistry of rock units at the potential repository level, Yucca Mountain, Nevada. *Appl. Geochem.* **17**, 683–698.

Raith, A., Perkins, W. T., Pearce, N. J. G. and Jeffries, T. E. (1996) Environmental monitoring on shellfish using UV laser ablation ICP-MS. Fresenius J. *Anal. Chem.* **355**, 789–792.

Russo, R. E., Mao, X. L., Borisov, O. V. and Liu, H. C. (2000) Laser ablation in atomic spectroscopy. *Encyclopedia of Analytical Chemistry: Instrumentation and Applications* (Meyers, R. A., ed.), 9485–9506, John Wiley & Sons Ltd., Chichster.

Russo, R. E., Mao, X. L., Liu, H. C., Gonzalez, J. and Mao, S. S. (2002) Laser ablation in analytical chemistry—A review. *Talanta* **57**, 425–451.

Russo, R. E., Mao, X. L., Liu, C. and Gonzalez, J. (2004) Laser assisted plasma spectrochemistry: laser ablation. *J. Anal. At. Spectrom.* **19**, 1084–1089.

Sela, H., Karpas, Z., Zoriy, M., Pickhardt, C. and Becker, J. S. (2007) Biomonitoring of hair samples by laser ablation inductively coupled plasma mass spectrometry (LA-ICP-MS). *Intern. J. Mass Spectrom.* **261**, 199–207.

Shepherd, T. J. and Chenery, S. R. (1995) Laser ablation ICP-MS elemental analysis of individual fluid inclusions—An evaluation study. *Geochim. Cosmochim. Acta* **59**, 3997–4007.

Šimůnek, J., van Genuchten, M. Th. and Šejna, M. (2005) The Hydrus-1D software package for simulating the one-dimensional movement of water, heat, and multiple solutes in variably-saturated media. Version 3.0, HYDRUS Software Series 1, University of California-Riverside, Riverside, CA, 270 pp.

Sylvester, P. J. (2005) Laser ablation ICP-MS developments and trends for 2003. *Geostand. Geoanal. Res.* **29**, 41–52.

Sylvester, P. J. (2008) LA-(MC)-ICP-MS trends in 2006 and 2007 with particular emphasis on measurement uncertainties. *Geostand. Geoanal. Res.* **32**, 469–488.

Tabatabai, M. A. and Sparks, D. L. (2005) *Chemical Processes in Soils*. Soil Science Society of America, Madison, Wisconsin.

Tanaka, K., Takahashi, Y. and Shimizu, H. (2007). Determination of rare earth element in carbonate using laser-ablation inductively-coupled plasma mass spectrometry: An examination of the influence of the matrix on laser-ablation inductively-coupled plasma mass spectrometry analysis. *Anal. Chim. Acta* **583**, 303–309.

Veinott, G. (2001) The use of laser ablation-ICP-MS in the environmental sciences. *Laser-Ablation-ICP-MS in the Earth Sciences: Principles and Applications* (Sylvester, P., ed.), vol. 29, 213–224, Mineralogical Association of Canada.

Wang, C. F., Chin, C. J., Luo, S. K. and Men, L. C. (1999) Determination of chromium in airborne particulate matter by high resolution and laser ablation inductively coupled plasma mass spectrometry. *Anal. Chim. Acta* **389**, 257–266.

Wang, H. A. O., Grolimund, D., Van Loon, L. R., Barmettler, K., Borca, C. N., Aeschimann, B. and Günther, D. (2011) Quantitative chemical imaging of element diffusion into heterogeneous media using Laser Ablation Inductively Coupled Plasma Mass Spectrometry, Synchrotron Micro-X-ray Fluorescence, and Extended X-ray Absorption Fine Structure Spectroscopy. *Anal. Chem.* **83**, 6259–6266.

Watmough, S. A., Hutchinson, T. C. and Evans, R. D. (1998) Development of solid calibration standards for trace elemental analyses of tree rings by laser ablation inductively coupled plasma-mass spectrometry. *Environ. Sci. Technol.* **32**, 185–2190.

Woodhead, J., Hellstrom, J., Paton, C., Hergt, J., Greig, A. and Maas, R. (2008) A guide to depth profiling and imaging applications of LA-ICP-MS. *Laser-Ablation-ICP-MS in the Earth Sciences: Current Practices and Outstanding Issues* (Sylvester, P., ed.), vol. 40, 135–145, Mineralogical Association of Canada.

Zhang, P. C. and Brady, P. V. (2002) Introduction to properties, sources and characteristics of soil radionuclides. Geochemistry of Soil Radionuclides (Zhang, P. C. and Brady, P. V., eds.), 1–20, SSSA Special Publication.